

A STUDY ON PROBABILISTIC EVALUATION OF SOIL LIQUEFACTION

By

Y. Yao Chi* and Li Ting Ou

Department of Land Management and Development

Chang Jung Christian University

396 Chang Jung Rd., Sec.1 Kway Jen, Tainan, Taiwan, R.O.C.

Ph:(886)06-2785123#2317; Fax:(886)06-2785902

E-mails: yunyao@mail.cju.edu.tw(Chi); ivy@ms65.url.com.tw (Ou)

*Corresponding author

Submitted to

Special issue on soil liquefaction

Soil Dynamics and Earthquake Engineering

December 2003

ABSTRACT

In the present study, a new method for evaluating annual liquefaction probability was developed based on both Davies and Berrill's seismic energy dissipation theory and Juang et al.'s limit state methodology. The new method also involves use of the average annual liquefaction probability (AALP) of divided soil layers to represent the AALP at a site. The developed method is illustrated in a case study where the AALP in Yunlin, a town that suffered from widespread liquefaction in the 1999 Chi-Chi earthquake, is assessed and mapped. The results show that high AALP area is located between south of County road No.148 and west of County road No.137, where the AALP is approximately equal to 0.01, indicating the cycle of liquefaction is about 100 years. The distribution of liquefaction probability is also discussed in this paper.

Key words: liquefaction evaluation, probability, seismic energy dissipation, earthquake.

1. INTRODUCTION

The 1999 Chi-Chi, Taiwan, earthquake caused a great destruction to this island country. One of the causes for the heavy damages to buildings, lifeline systems, and harbor facilities is the widespread liquefaction induced by the Chi-Chi earthquake. Therefore, evaluation of soil liquefaction potential has become one of the most important geotechnical earthquake engineering topics of interest in Taiwan. Because of the difficulty and the high cost in obtaining the high-quality undisturbed samples, simplified methods based on *in situ* tests such as the standard penetration test (SPT) and the cone penetration test (CPT) are preferred by the geotechnical engineer to evaluate earthquake-induced liquefaction potential (Seed et al.[1]; Robertson and Wride [2]).

The occurrence of initial liquefaction is often vague due to the uncertainty of earthquake parameters including earthquake magnitude, closest distance to the epicenter and earthquake duration, and the uncertainty of soil parameters including the unit weight and strength characteristics of the soil. Moreover, the safety factors in the traditional liquefaction potential analysis are often difficult to interpret because of these uncertainties. To deal with the uncertainties, probabilistic and statistical approaches have been employed. For example, Haldar and Tang [3] performed second-moment analysis of the SPT-based limit state that was established by Seed and Idriss [4]. Liao et al [5] employed statistical regression methods to quantify the probability of liquefaction as a function of given earthquake load and the SPT resistance. Juang et al. [6] used the advanced first-order second-moment (AFOSM) techniques to calculate the reliability index and to map it to the probability of

liquefaction. Lee [7] used the first-order second-moment (FOSM) method to develop a procedure for estimating the probability of liquefaction, which was based on the SPT- and CPT-based simplified methods.

Soil liquefaction often follows the earthquake immediately. As a result, an earthquake may be seen as an energy dissipation behavior (Nasser and Shokooh [8]; Davis and Berrill [9]). Davis and Berrill [9] developed an energy method to assess soil liquefaction. Juang et al. [10] used Artificial Neural Network (ANN) technology to develop limit state for liquefaction evaluation. Recently, a new method for evaluating annual liquefaction probability (ALP) was developed on the basis of both Davies and Berrill's seismic energy dissipation theory and Juang et al.'s limit state approach (Chi, et al. [11]).

Iwasaki et al. [12] proposed a procedure to evaluate liquefaction potential index, which was based on the in situ test data over the entire borehole (or more accurately, the top 20 m). The liquefaction potential was integrated over the depth using a weighted average scheme. However, the liquefaction potential index defined by Iwasaki et al. [12] is not a probability. In this paper, the new method by the writers [11, 13] is further developed, and used to map the liquefaction potential of the Yuanlin area using the Chi-Chi earthquake parameters.

2. THE MODEL DEVELOPMENT

There are two classes of assumptions on the excess pore pressure in the liquefied soil. The first assumption relates the excess pore pressure to the shear stresses generated by the ground shaking. The second one relates the excess pore

pressure to the amount of seismic energy dissipated in the soil. In this paper, the second assumption is employed.

Seismic Energy Dissipation Model

The advanced seismic energy dissipation model is used to calculate the liquefaction probability in this study. The energy content of the seismic wave arriving at the site of interest is assumed to come from the total radiated energy of the earthquake. In addition, the distance to the center of energy release and the portion of arriving energy are assumed to depend upon the SPT-N value and the initial effective overburden stress. The seismic energy dissipation model is to explain the simple relationship giving the increase in excess pore pressure and is believed to be a function of (1) the earthquake magnitude, (2) its distance from the site, (3) the SPT-N value, and (4) the initial effective overburden stress. Symbolically,

$$\frac{\Delta u}{\sigma_v'} = f(M, R, N_1, \sigma_v') = \frac{A \cdot 10^{1.5M}}{R^B N_1^C \overline{\sigma_v'}^D} \dots\dots\dots(1)$$

where Δu is the excess pore pressure, A, B, C and D are the constants, M is the earthquake magnitude, R is the distance from the site to the energy release center in kilometer, N_1 is the stress corrected SPT-N value, and $\overline{\sigma_v'}$ is the effective overburden stress in kpa. When the ratio of the excess pore pressure to the effective overburden stress equals to one, the soil liquefaction occurs. As a result, Equation (1) can be rewritten as:

$$1.5M = \log(1/A) + B \log R + C \log N_1 + D \log(\bar{\sigma}_v') \dots\dots\dots(2)$$

Annual Liquefaction Probability

The annual liquefaction probability (ALP) is defined and formulated in the paragraphs that follow.

The annual number of earthquakes n where their magnitude M exceeds a given magnitude m can be estimated by the Gutenberg and Richter's [14] method:

$$\log(n) = \log(T) - b m \dots\dots\dots(3)$$

where T represents the total annual number of earthquakes with positive magnitude and b describes the relative likelihood of large and small earthquakes. From this equation we have

$$P[M \geq m] = \frac{n}{T} = 10^{-bm} \dots\dots\dots(4)$$

Combining Equation (1) with Equation (4) gives

$$P[\Delta u / \sigma_v' \geq 1] = P[M \geq (2/3) \log(R^B N_1^C \bar{\sigma}_v'^D / A)] = \left[R^B N_1^C \bar{\sigma}_v'^D / A \right]^{-\frac{2}{3}b} \dots\dots (5)$$

Based on the Davies and Berrill's concept of cumulative probability of liquefaction, we can integrate over the length of the fault, where a uniform probability of earthquake

occurrence is assumed along the fault. The integration will result in the following form:

$$P\left[\frac{\Delta u}{\bar{\sigma}_v'} \geq 1\right] = \frac{\pi}{L} \left[N_1^c \bar{\sigma}_v^D / A \right]^{\frac{2b}{3}} \cdot \frac{\Gamma(\gamma)}{(2R_{mid})^\gamma \left[\Gamma\left(\frac{\gamma+1}{2}\right) \right]^2} \dots\dots\dots(6)$$

where $r = (2/3)Bb - 1$ and $\Gamma(\gamma)$ is the Gamma function. Finally, assuming the occurrence of earthquakes along the fault is viewed as a Poisson process, the ALP is given by

$$P_f = 1 - \exp\left(-TP\left[\frac{\Delta u}{\bar{\sigma}_v'} \geq 1\right]\right). \dots\dots\dots(7)$$

Combining Equation (6) with Equation (7) gives

$$P_f = 1 - \exp\left\{ -\pi \left(\frac{T}{L} \right) \left[N_1^c \bar{\sigma}_v^D / A \right]^{\frac{2b}{3}} \cdot \frac{\Gamma(\gamma)}{(2R_{mid})^\gamma \left[\Gamma\left(\frac{\gamma+1}{2}\right) \right]^2} \right\}, \dots\dots\dots(8)$$

where T is the total annual number of earthquakes with positive magnitude, L is the length of the fault in kilometer, T/L is the number of positive magnitude earthquakes

per year per unit length of the fault, and R_{mid} is the distance from the site to the midpoint of the linear fault as shown in Fig.1.

Equation (8) represents the annual liquefaction probability (ALP) for each soil layer caused by unitary fault. For a system with N independent faults, the ALP may be estimated with the following equation, which is based on reliability theory [15]:

$$p(f) = 1 - \prod_{i=1}^N (1 - p_i). \quad \dots\dots\dots(9)$$

where p_i is the ALP caused by fault i , and $p(f)$ is the probability of liquefaction.

The next step in the analysis is to determine the average annual liquefaction probability (AALP) using the data of the entire borehole. One possibility to integrate all ALPs for individual layers caused by each fault into the AALP is to use some weighted average scheme such as the one proposed by Iwasaki et al. [12]. In this study, we compute the AALP using the divided sandy layers approach within the depth of 20 m. The procedure is described later.

The Constants

The constants in Equation 2 need to be determined empirically before the calculation of the ALP and the AALP. Conceptually, Equation 2 represents a limit state function. A database of 94 field cases, including 48 liquefied cases and 46 non-liquefied cases, compiled by Tokimatsu and Yoshimi [16], is used to define the limit state of liquefaction. For each case, a search technique developed by Juang et al. [10] is used to search for a *critical* peak ground surface horizontal acceleration (a_{max})

where the factor of safety (F_S) calculated with the SPT-based simplified method [17] is equal to 1. For a liquefied case, this involves a reduction in the seismic loading (i.e., a_{\max}) so as to raise the calculated F_S to 1.0^+ , indicating no liquefaction. For a non-liquefied case, the process involves an increase in the seismic loading (i.e., a_{\max}) so as to decrease the calculated F_S to 1.0^- , indicating liquefaction. The search technique is illustrated in Figure 2.

The relation by Campbell [18] is then used to determine the distance to epicenter R for the “point” on the limit state surface resulting from the search:

$$a_{\max} = 0.0185e^{1.28M} [R + 0.147e^{-0.732M}]^{-1.75} \dots\dots\dots(10)$$

The 94 case histories each with the adjusted seismic loading are then used to develop the limit state of liquefaction resistance through non-linear regression analysis:

$$1.5M = \log 1/0.004236 + 3.2441 \log R + 1.106 \log N_1 + 0.974 \log \overline{\sigma}_v, \dots(11)$$

Figure 3 shows the data points for the regression, with $R^2 = 0.89$. Comparing Equation (11) to Equation (2), one can obtain $A = 0.001236$, $B = 3.244$, $C = 1.106$, and $D = 0.974$. These constants can be used with Equation (8) to compute the annual probability of liquefaction of each soil layer.

Figure 4 shows a plot of the 94 cases in the coordinates of Figure 3. The straight line in Figure 4 is the limit state line represented by Equation 11. Most liquefied data points are located above the line, and most non-liquefied data points are

located below the line. Some scatter of the liquefied and non-liquefied data points is observed in Figure 4. The success rate in distinguishing liquefied and non-liquefied cases is 80%, which is about the same as the accuracy of using the SPT-based simplified method in this data set [17].

PROCEDURES FOR EVALUATING AALP

Evaluating AALP Based on Statistical Theory

Lee [7] presented the statistical analysis of the probability of liquefaction. The output of his model is the probability of liquefaction for a given earthquake. In this section, his method is extended with the formulation of AALP described in this paper. The procedure for evaluating AALP based on the statistical theory is summarized as follows:

1. Estimate earthquake magnitude and peak horizontal acceleration at the site of interest using the method developed by Chi et al. [13].
2. At each borehole, divide the soil profile into layers. For each layer, obtain representative soil parameters and the seismic parameters, and then calculate CSR and CRR using the SPT-based method described in Youd et al. [17].
3. Obtain the coefficient of variation (COV) of the variable CSR, Ω_D , the COV of CRR, Ω_C , respectively; and then calculate the probability of liquefaction P_f as follows:

$$Pf = P(C \leq D) = 1 - \phi(\gamma)$$

$$= 1 - \phi \left(\frac{\ln \left(\frac{\mu_C}{\mu_D} \times \sqrt{\frac{1 + \Omega_D^2}{1 + \Omega_C^2}} \right)}{\sqrt{\ln[(1 + \Omega_D^2)(1 + \Omega_C^2)]}} \right) \dots\dots\dots(12)$$

4. By means of Bayes' theorem (Harr[15]), the annual probability of liquefaction of each layer can be obtained from the conditional probability:

$$P[L] = P[L|M] \times P[M], \dots\dots\dots(13)$$

Where $P[L]$ is the annual probability of liquefaction, $P[L|M]$ is the conditional probability of liquefaction (when $P[L|M] = 0.46$, liquefaction is initiated) and $P[M]$ is the mean annual rate of exceeding magnitude m , which is also denoting as λ_m . The term λ_m can be obtained from a seismic hazard analysis.

5. The average annual liquefaction probability can be obtained from Equation (9), and its inverse yields the period of liquefaction.

Nothing has been edited below this point.

AALP Based on Seismic Energy Dissipation Model

The AALP of soils based on seismic energy dissipation model has been developed previously. Applying this model, the developed methodology involves the following steps:

Step1. Earthquake sources and parameters

The earthquake sources include both point source and linear source, for example generally originate in zones near the volcanoes that are small enough to allow them to be characterized as point sources, and in such a case the hazard analysis can be simplified with negligible loss of accuracy by approximating the planar source as a linear source zone. In Taiwan Western, earthquake source is linear source. Therefore, according to Taiwan Western geologic map by Central Geological Survey, MOEA, Taipei, Taiwan ROC., the location of Chelungpu fault and Zhanghua fault are both near the Yunlin area, the length of two faults is equal to 86km and 32km individually (Fig.5), where we would analysis following as an example to illustrate the developed methodology.

Cheng et al. [19] have developed the Taiwan earthquake sources zones and estimating the seismic parameters. The Yunlin area is located in the E earthquake source and the seismic parameter b is equal to 1.087, and another seismic parameter a, is equal to 4.348 (Chi et al. [13]). Thus, we can obtain following equation through the equation (3),

$$T = 10^{4.348} . \quad \dots\dots\dots(15)$$

Step2. Average annual probability of liquefaction

The above procedure creates seismic parameters that substitution equation (8) could obtain ALP of each soil layer. According to equation (9) could combine ALP of each soil layer based on different faults, and then calculated the AALP of divided soil layer to represented the hole liquefaction probability.

Step3. The above procedure creates the AALP that reciprocal is average return period of liquefaction (Eq.16).

$$t_L = P_L^{-1} \dots\dots\dots(16)$$

CASE STUDY

The 1999 Chi-Chi earthquake had a magnitude M_w of 7.6, and had caused extensive casualties and soil liquefaction in central Taiwan including Taichung, Nantou, Zhanghua, Yunlin, Jiayi. In this study, 45 bore logging records from Yunlin area, are obtained from the Moh and Associates Consulting Engineers Co. (MACE). The 45 case records include 15 cases of liquefied 11 cases of non-liquefied and 19 cases of unknown-liquefied. The location of water table is about 0.5~4m depth under ground surface in Yunlin area in 1999(MACE [20]).

Subsurface Soil Layer Characteristics in Yunlin Area

In this paper, the liquefaction probability of divided soil layers describes the subsurface conditions in Yunlin area. According to the bore logging data from MACE [20], there are five cross-sections shown in Fig. 6. These cross sections cut across the study area from west to east including three cross-sectional profiles and from north to south including two cross-sectional profiles. Subsurface soil layer conditions are illustrated by the five cross-sectional profiles shown in Fig.7~11.

The site is underlain by three layers of sand, the upper two layers about 2~15-m-thick, the depth of last sand layer do not be found. The depth of sand layer is more the larger quantity of SPT-N value, indicated that the strength of sand increasing

with depth. Fig. 7, 8 and 9 show the subsurface Conditions of profiles along with the section of A, B and C from west to east individually. The first sand layer (nearest ground surface) is disappeared by clay layer near the east at the A-section (BH-3 and BH-5). B section that located in south of A-section, in the west of the second sand layer is disappeared at BH-17, and becomes with interlayer of clay at BH-49. In the C-section profile, the first sand layer is disappeared at BH-43. The similarity between the D and E section from north to south shown in Fig. 10~11, that the near the south of clay layer were disappeared by sand. About the B and C section that at the south within the Yunlin area, so that the sand relatively thick for clay, and the appearance the same as D section and E section. According to five cross-sectional profiles the sand layer relatively thick for clay layer at the south slanted towards east of Yunlin area, and then the situation is oppositely at the south slanted towards west and north of Yunlin area. A roughly within 20 depths that the sand and clay interlace, that could divide three layers of sand, called surface sand layer, second sand layer and third sand layer individually.

The Results of the Seismic Energy Dissipation Model

As described in the last section, the evaluation of liquefaction probability of soils based on seismic energy dissipation model is developed. In this section, it is sensible to discuss the use of 45 input case records to yield the AALP based on Chelungpu fault and Zhanghua fault shown in Table 1. It not only shows that the AALP of surface sand layer is liquefied usually damages the surface structures, but also shows that it be ranked by decreasing value of AALP on Chelungpu fault for comparing to the in-situ liquefied area of Chi-Chi earthquake. The AALP based on

Zhanghua fault is greater than one based on Chelungpu fault. Owing to the Zhanghua fault that within the Yunlin area, therefore, the distance from site to fault is one of reasons. Six data points, BH-41, -12, -27, -7, -25 and -43 are particularly bothersome in that they appear to contradict the investigation results after Chi-Chi earthquake. Roughly, the developed model yields an overall success rate of 87% in predicting both liquefied and non-liquefied tendency. The combined AALP with both faults shows in Fig. 7~11, as denoted cross sign curves at the location of boring holes. These are points including BH-41, -12 and -7, where the liquefaction appearance of sand layer did not be observed because of existing a 2~6-m-thick clay layer upon surface sand layer. The location of BH-27 is between the location of BH-26 and BH-29 in D and E section individually. Because of BH-26 and -29 are both liquefied, similar condition could exist at BH-27. According to Fig.9, the surface sand layer is underlain an upper soil layer about 10-m-thick at BH-25 and -43. The soil of upper layer is clay or clayey silt with low liquefaction potential. In summary, the results of the developed method are in good agreement with the investigation results in Chi-Chi earthquake.

A Comparison of the Seismic Energy Dissipation Model to the Statistical Model

In a typical field investigation, the sites that have no evidence of liquefaction are less likely to investigate. Thus, the verification of a liquefaction probability model is difficult. The results similarly show that the AALP obtained from the two different models, and then in this study, the AALP calculated by seismic energy dissipation model compared to that calculated by statistical model. The mapping of relationship about the AALP of surface layer of two models that based on divided soil layer that

shown in Fig.12. Show the result of the probability of seismic energy dissipation model has a higher degree of relation with statistical model ($R^2 = 0.71$). Most data points are below the diagonal, which indicated that the results by statistical mode are lager then ones obtained by energy dissipation model. Thus, the results using the developed method (energy dissipation model) are conservatively.

The Map of AALP Based on the Seismic Energy Dissipation Model

The natural disasters evaluation must consider the element of whole that could compare to other natural disasters. Therefore using the above evaluation steps, we can calculate the AALP and the average return period of liquefaction for the divided soil layer (shown in Table 2), and mapping the results for Yunlin area (shown in Fig.13).

Table 2 shows that the AALP of the surface sand layer is greater than the second sand layer, and the results conform to the generally assumption. Besides, Table 2 shows the AALP of over hole based on depth weighted averages method developed by Iwasaki [12] that can fine the results, which one smaller than the second sand layer, since the results expressed in index of liquefaction not in liquefaction probability.

Fig. 13 shows the map of AALP for Yunlin area that result shown the high AALP area was between south of county road No.148 and west of county road No.137, that AALP was approximately 0.01 and the average return period of liquefaction was approximately 100 years.

According to the liquefaction analysis and remediation in Yuanlin area by Wen [21], the Lunya neighborhood was the most remediation that shows great destruction of liquefaction at here in the 921 earthquake. Hence, using the map of AALP as compared with 45 case records can be fined including BH-20, -21, -23, -28, -29, -30,

-35, -43, -46, -47 and -48 altogether 12 case records in Lunya neighborhood. The 12 case records have 6 case records AALP equal or greater than 0.01 and the average return period of liquefaction within 100 years. Other seven case records including BH-20, -23, -34 and -48, besides BH-30 and BH-43 that identified as unknown-liquefaction from MACE [20] by SPT in the 921 earthquake. The BH-43 has a clay layer of quite thickness that equal 8 m from surface and the water table at 0.5 m. To base on the above-mentioned that discovered the points of liquefied of the AALP equal or greater than 0.01 in the 921 earthquake, therefore, the average return period of liquefaction approximately 100 years in Yunlin area.

CONCLUSIONS

1. A new framework for the average annual liquefaction probability (AALP) is developed in this paper. The method is implemented in a spreadsheet and, given the SPT profiles. Thus, the profile of the probability of liquefaction can be easily obtained.
2. The AALP of the surface sand layer is greater than the second sand layer, which conform to the general assumption.
3. The results indicate that our model has a higher degree of relation to the statistical model. The results of the developed method are conservatively.
4. Our results show that Lunya neighborhood has the highest AALP, and these results are similar to previous investigation results after the Chi-Chi earthquake. The developed model yields an overall prediction rate of 87% in both liquefied and non-liquefied tendency.

5. The map of AALP in Yunlin area shows that the high AALP area is located between south of county road No.148 and west of county road No.137, where the AALP is approximately 0.01 indicating that the average return period of liquefaction is about 100 years.

ACKNOWLEDGMENTS

This study is sponsored by the National Science Council (NSC) in Taiwan recorded Grant No. NSC-91-2211-E-309-004. The authors particularly to thank to professor Lee, D.H., professor Huang, A.B. and professor Hsieh, B.B. for their comments on this study.

REFERENCES

- [1] Seed, H. B., Tokimatsu, K. Harder, L. F., and Chung, R. M., " Influence of SPT procedures in soil liquefaction resistqnce evaluation", Journal of Geotechnical Engineering, ASCE, Vol. 111, No. 12, pp. 1425-1445, 1985.
- [2] Robertson, P. K., and Wride, C. E., " Evaluation cyclic liquefaction potential using the cone penetration test," Canadian Geotechnical Journal, Vol. 35, pp. 442-459, 1998.
- [3] Haldar, A., and Tang, W. H., " Probabilistic evaluation of liquefaction potential," Journal of Geotechnical Engineering Division, ASCE, Vol. 105, No. GT2, pp. 145-162, 1979.
- [4] Liao, S. S., and Veneziano, D., and Whitman, R. V., " Regression model for evaluating liquefaction probability, " Journal of Geotechnical Engineering, ASCE, Vol. 114, No. 4, PP. 389-411, 1988.
- [5] Seed, H. B., and Idriss I. M., "Simplified procedure for evaluating soil liquefaction potential," Journal of Geotechnical Engineering, ASCE, Vol. 97, pp.1249-1273, 1971.
- [6] Juang, C. H., Rosowsky D.V. and Tang, W.H., "Reliability-based method for assessing liquefaction potential of soils," Journal of Geotechnical and Geoenvironmental Engineering, PP. 684-689, 1999.
- [7] Lee, Y.F., "The Study on Probabilistic in Evaluation Method of Seismic Liquefaction," M. D. Dissertation, Department of Land Management and Development, Chang Jung Christian University, Taiwan, Tainan, 2001.

- [8] Nasser, S. N., and Shokooch, A., "A unified approach to densification and liquefaction of cohesionless sand in cyclic shearing," *Journal of Canadian Geotech*, vol. 16, pp.659-678, 1979.
- [9] Davis, R.O. And Berrill, J.B., "Energy dissipation and seismic liquefaction in sands," *Earthquake Engineering and Structural Dynamics*, Vol. 10, pp.59-68, 1982.
- [10] Juang, C.H., Chen, C.J., Jiang, T., and Andrus, D, "Risk-based liquefaction potential evaluation using standard penetration test, " *Can. Geotech. Journal*, Vol.37, pp. 1195~1208, 2000.
- [11] Chi, Y. Y., Ou, L. T., and Chen, Y. R., "The liquefaction probability model via seismic energy dissipation theory," *The 10th conference on current research in geotechnical engineering in Taiwan*, Sanshia, 2003.
- [12] Iwasaki, T., Arakawa, T., and Tokida, K., "Simplified procedures for assessing soil liquefaction during earthquakes", *Soil Dynamics and Earthquake Engineering Conference Southampton*, pp.925-939, 1982
- [13] Chi, Y. Y., Ou, L. T., and Chen, Y. R., "Probability-based method for assessing liquefaction potential of soils," *A probabilistic approach in assessing the liquefaction potential*, Taiwan, Tainan, 2003.
- [14] Gutenberg, B. and Richter, C.F., "Seismicity of the earth," *Princeton University Press*, 1954.
- [15] Harr, M. E., *Reliability-Based Design in Civil Engineering*, McGraw-Hill, New York, 1987.

- [16] Tokimastu, K. and Yoshimi, Y., " Empirical correlation of soil liquefaction based on SPT-N Value and fines content," Soil and Foundations, Vol. 23, No. 4, pp. 56-74, 1983.
- [17] Youd, T. L., and Idriss, I. M., "Proceeding of the NCEER workshop on evaluation of liquefaction resistance of soils", Salt Lake, 1997.
- [18] Campbell, K.W., "Near source attenuation of peak horizontal acceleration, " Bulletin of the Seismological Society of America, Vol.71, pp.2039-2070, 1981.
- [19] Cheng, C. T., Lee, C.T., and Tsai, Y. B., "Seismic Hazard Analysis Assisted By A Geographic Information System," Sino-Geotechnics , No. 69, pp.41-50, 1998.
- [20] Moh and Association, INC., " The Research of Soil Liquefaction Conducted in the areas of Yunlin and Dacun," National Science Council, 2000.
- [21] Wen, H.Y., "The Application of GIS in Liquefaction Analysis and Remediation in Yuanlin," M. D. Dissertation, Department of Civil Engineering, National Central University, Taiwan, 2002.

Table 1 The AALP and the Return Period for Two Faults

Hole No.	AALP		Return period(year)		Site investigation
	Chelungpu fault	Zhaughua fault	Chelungpu fault	Zhaughua fault	
BH-21	0.006320	0.026479	158	38	Y
BH-41	0.006159	0.026115	162	38	N
BH-9	0.003936	0.013692	254	73	NA
BH-13	0.003151	0.012012	317	83	NA
BH-12	0.003037	0.011864	329	84	N
BH-18	0.002959	0.014985	338	67	Y
BH-44	0.002857	0.014173	350	71	Y
BH-27	0.002835	0.015709	353	64	N
BH-22	0.002694	0.010509	371	95	NA
BH-49	0.002498	0.011295	400	89	NA
BH-5	0.002496	0.006552	401	153	Y
BH-3	0.002475	0.007123	404	140	Y
BH-7	0.002444	0.008541	409	117	N
BH-46	0.002384	0.012189	419	82	Y
BH-45	0.002342	0.011931	427	84	Y
BH-28	0.002281	0.012117	438	83	Y
BH-19	0.002233	0.010282	448	97	NA
BH-50	0.002142	0.010186	467	98	NA

BH-29	0.002055	0.010510	487	95	Y
BH-26	0.001900	0.010749	526	93	Y
BH-42	0.001831	0.007872	546	127	NA
BH-47	0.001810	0.009869	552	101	Y
BH-30	0.001788	0.007849	559	127	Y
BH-35	0.001761	0.009302	568	108	Y
BH-31	0.001744	0.010544	573	95	N
BH-15	0.001703	0.007294	587	137	N
BH-11	0.001482	0.006209	675	161	NA
BH-25	0.001461	0.007825	684	128	Y
BH-48	0.001426	0.006976	701	143	NA
BH-1	0.001320	0.003685	758	271	NA
BH-24	0.001296	0.006885	771	145	NA
BH-34	0.001192	0.007318	839	137	NA
BH-6	0.001060	0.004069	944	246	NA
BH-23	0.001037	0.004690	964	213	NA
BH-8	0.001020	0.003202	980	312	NA
BH-33	0.000945	0.006339	1059	158	NA
BH-10	0.000900	0.003888	1112	257	N
BH-2	0.000840	0.002030	1191	493	NA
BH-43	0.000759	0.003683	1317	272	Y
BH-14	0.000727	0.002575	1375	388	N

BH-20	0.000507	0.002399	1973	417	NA
BH-17	0.000505	0.002397	1980	417	N
BH-32	0.000459	0.002866	2177	349	N

Note. N is mean non-liquefied; Y is mean liquefied; NA is mean unknown

TABLE 2. AALP and Return period Based on Seismic Energy Dissipation Model

Hole No.	Surface sand layer		Second sand layer		Iwasaki ^a		Site ^b investigation
	AALP	Return period	AALP	Return period	AALP	Return period	
BH-21	0.032631	31	0.006151	163	0.005952	168	Y
BH-41	0.032114	31	0.004874	205	0.003913	256	N
BH-27	0.018497	54	0.004442	225	0.007863	127	N
BH-18	0.017898	56	0.004884	205	0.007272	138	Y
BH-9	0.017575	57	0.002759	362	0.002650	377	NA
BH-44	0.016990	59	0.004822	207	0.004414	227	Y
BH-13	0.015125	66	0.003603	278	0.004958	202	NA
BH-12	0.014865	67	-	-	0.002571	389	N
BH-46	0.014544	69	0.021557	46	0.006949	144	Y
BH-28	0.014370	70	0.005316	188	0.005234	191	Y
BH-45	0.014245	70	0.003547	282	0.004843	207	Y
BH-49	0.013765	73	0.003381	296	0.005139	195	NA
BH-22	0.013166	76	-	-	0.006099	164	NA
BH-26	0.012628	79	0.005824	172	0.006331	158	Y
BH-29	0.012541	80	0.003416	293	0.005290	189	Y
BH-19	0.012491	80	0.010884	92	0.004345	230	NA
BH-50	0.012306	81	0.003956	253	0.002520	397	NA
BH-31	0.012268	82	0.007424	135	0.004776	209	N
BH-47	0.011657	86	0.003325	301	0.007303	137	Y
BH-35	0.011045	91	0.003691	271	0.003849	260	Y
BH-7	0.010965	91	0.003422	292	0.001942	515	N
BH-42	0.009689	103	0.005125	195	0.003240	309	NA
BH-30	0.009621	104	0.002642	379	0.004780	209	Y
BH-3	0.009580	104	0.002243	446	0.001535	652	Y
BH-25	0.009275	108	0.004598	217	0.002140	467	Y
BH-5	0.009033	111			0.001335	749	Y
BH-15	0.008982	111	0.002772	361	0.003882	258	N
BH-34	0.008501	118	0.004144	241	0.003224	310	NA
BH-48	0.008392	119	0.002964	337	0.001237	809	NA
BH-24	0.008172	122	0.003651	274	0.002924	342	NA
BH-11	0.007681	130	0.004581	218	0.002090	479	NA
BH-33	0.007275	137			0.004257	235	NA
BH-23	0.005722	175	0.003731	268	0.002730	366	NA
BH-6	0.005124	195	0.003441	291	0.002676	374	NA
BH-1	0.005000	200	0.002780	360	0.001224	817	NA

BH-10	0.004784	209			0.001854	539	N
BH-43	0.004439	225	0.004619	216	0.001952	512	Y
BH-8	0.004218	237	0.002267	441	0.002604	384	NA
BH-32	0.003324	301	0.003547	282	0.001347	742	N
BH-14	0.003300	303			0.003512	285	N
BH-20	0.002905	344	0.002329	429	0.001620	617	NA
BH-17	0.002900	345			0.000940	1064	N
BH-2	0.002868	349			0.000369	2713	NA

Note. a: the AALP of over hole based on depth weighted averages method by Iwasaki

b: N is mean non-liquefied ; Y is mean liquefied; NA is mean unknown

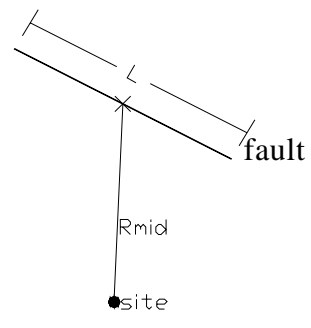


Fig. 1 Linear Fault and Potential Liquefaction Site

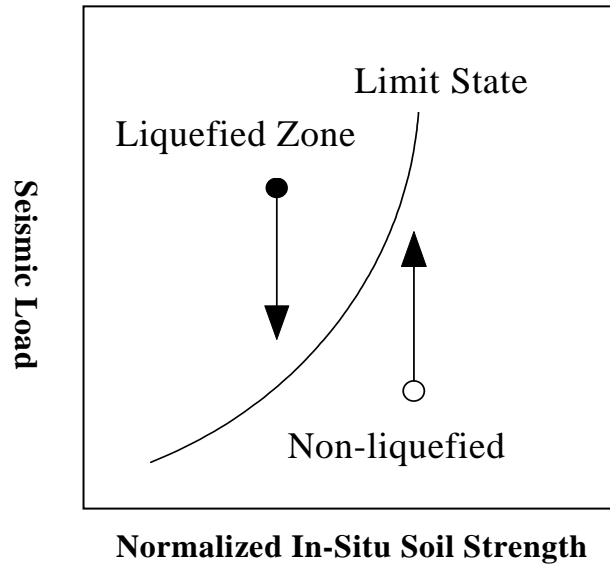


Fig. 2. Liquefaction/Non-liquefaction of Limit State Boundary

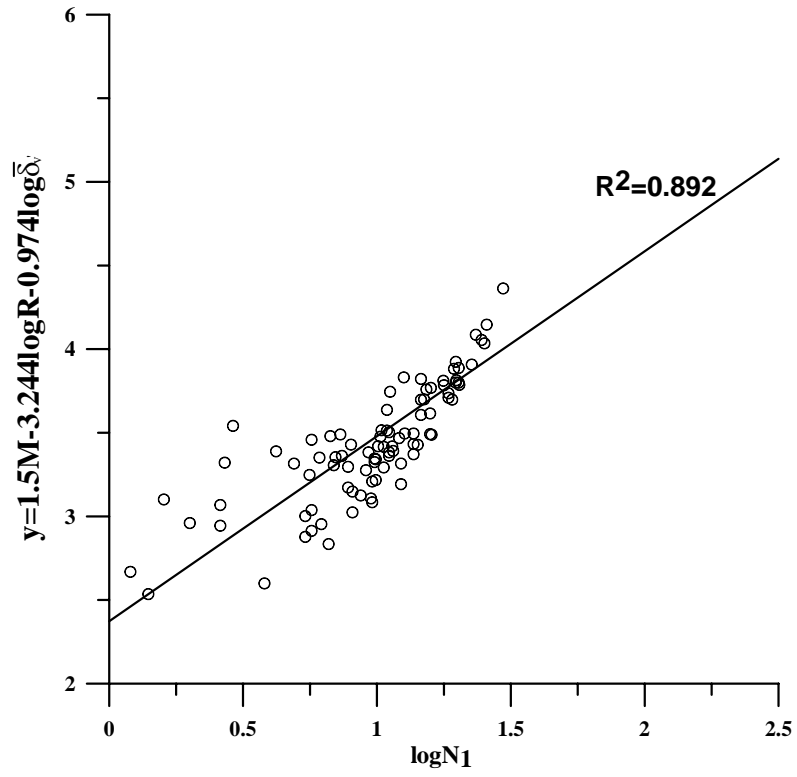


Fig. 3 Limit State Boundary Regressed by Initial Liquefaction Data.

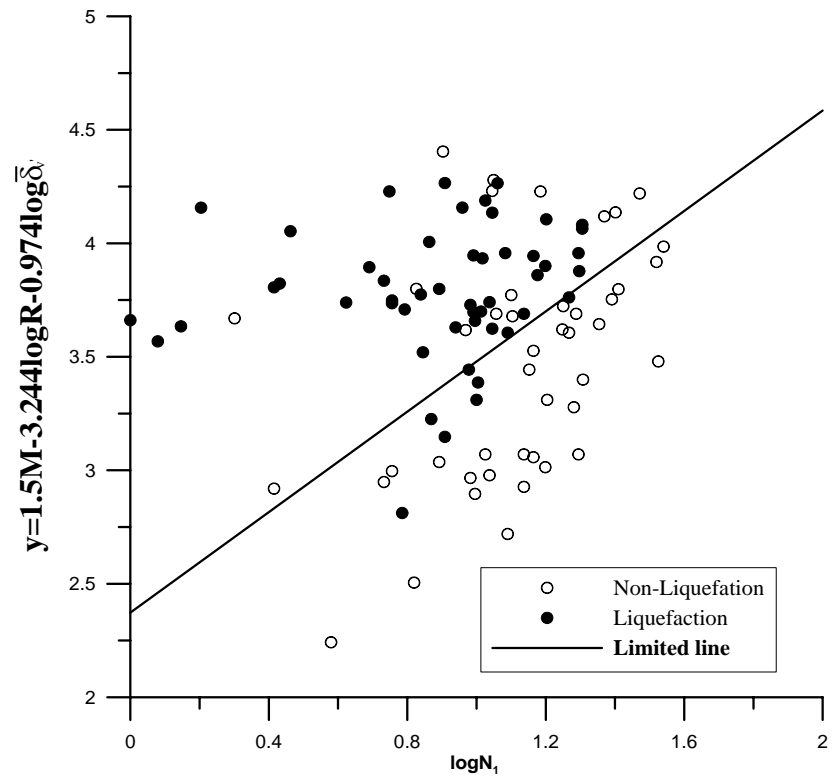


Fig.4 The Historical Records Divided by Limit State Boundary

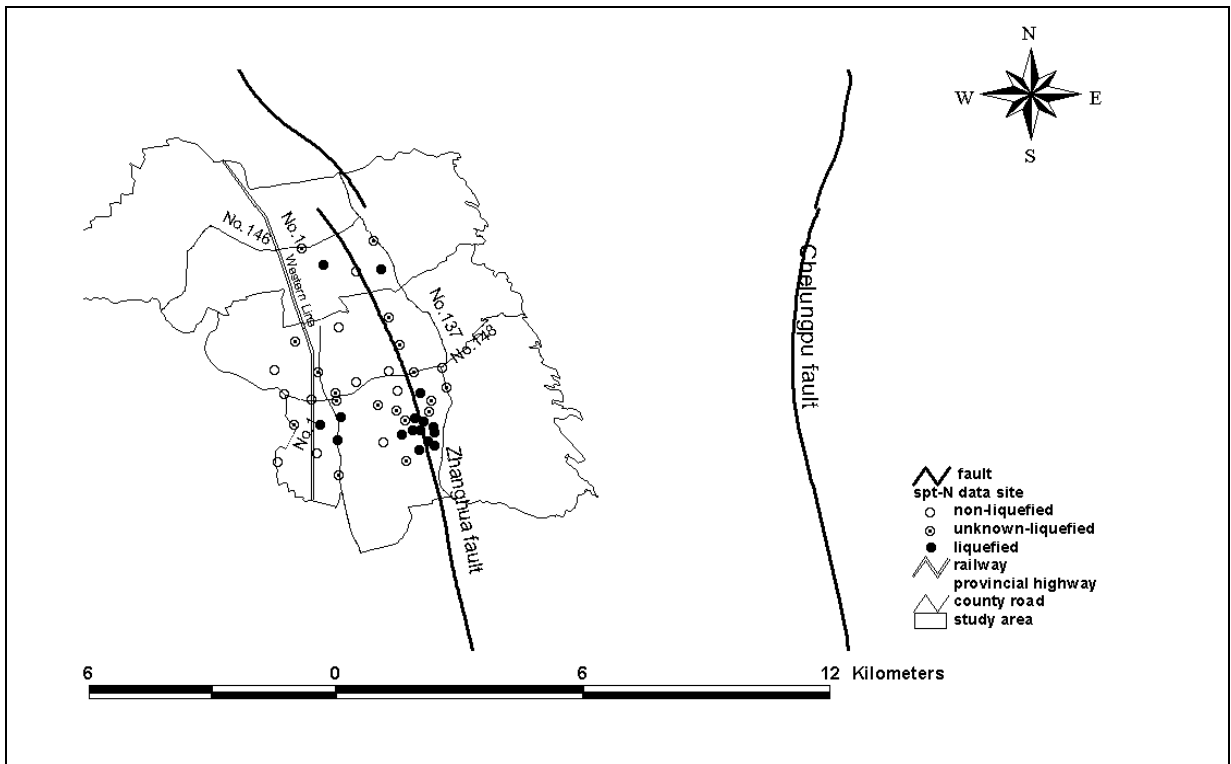


Fig. 5. Location Map for Fault Site

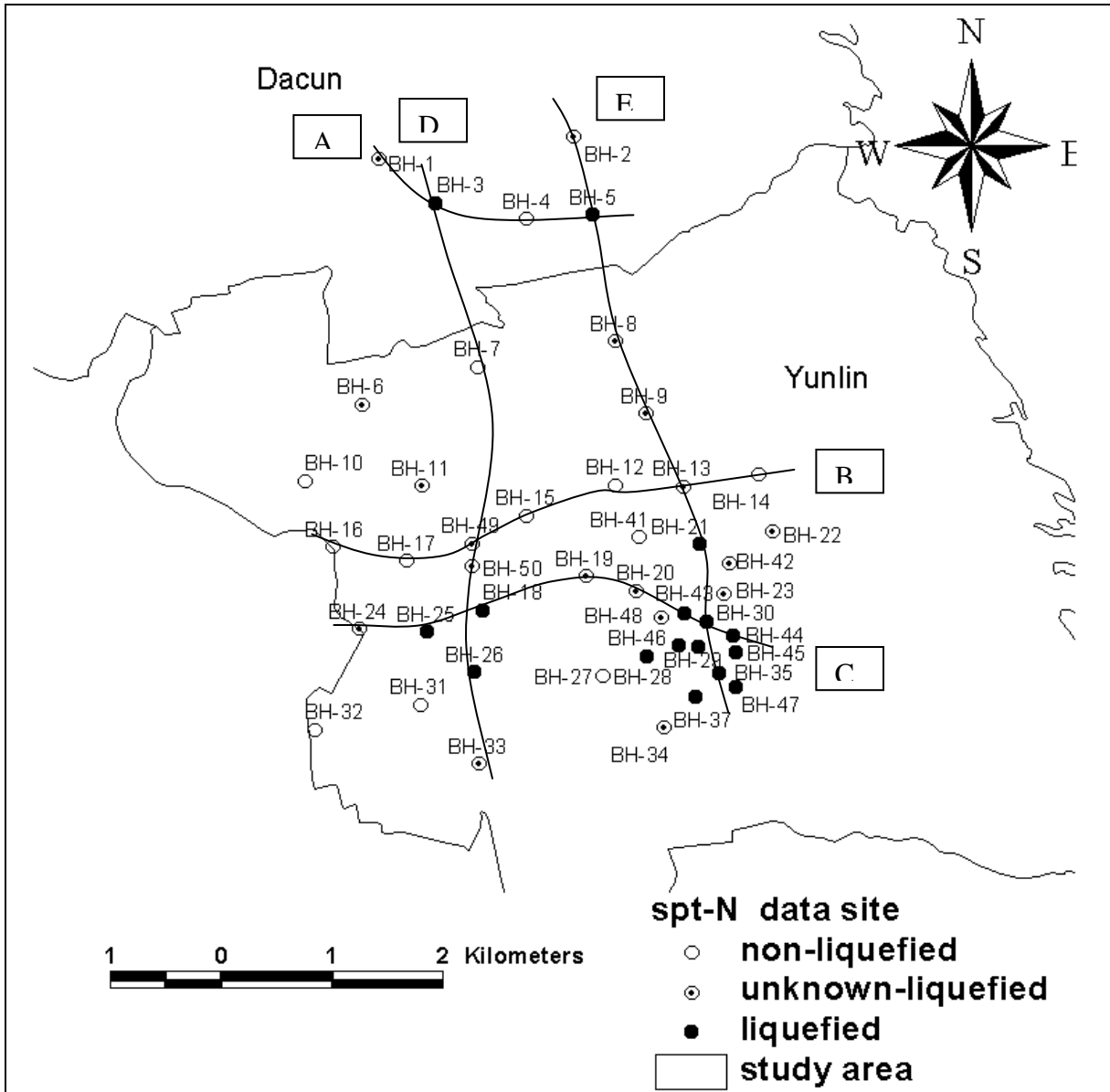


Fig. 6. Location Map for SPT Boring Holes and Cross-Sections through Map Zone

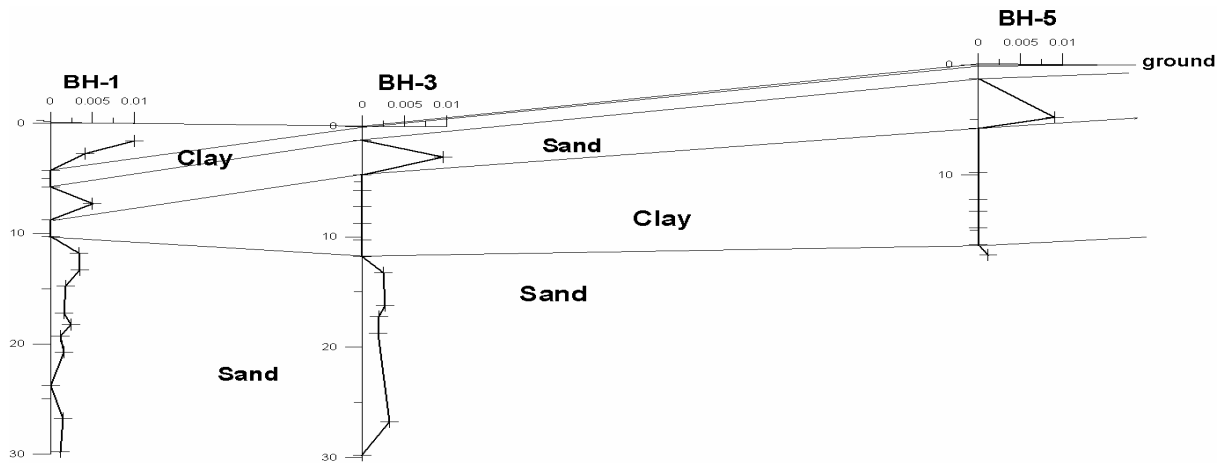


Fig. 7. The Soil and ALP Profile of A Section

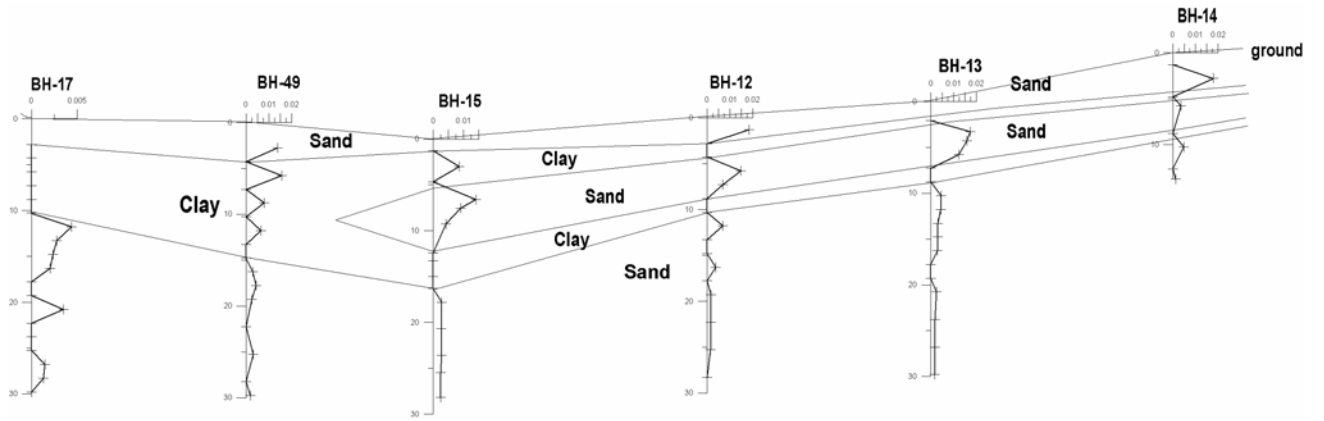


Fig. 8. The Soil and ALP Profile of B Section

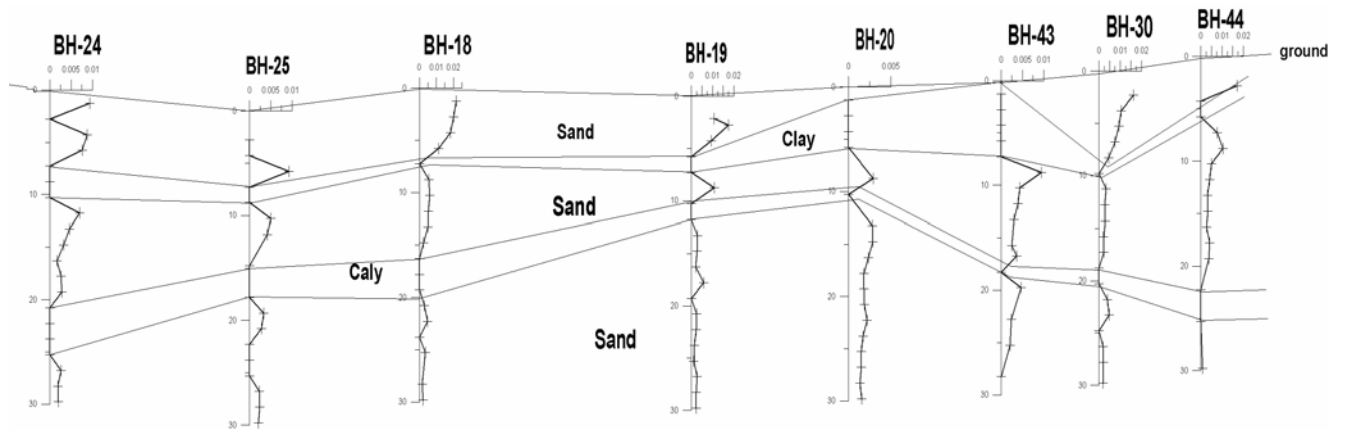


Fig. 9. The Soil and ALP Profile of C Section

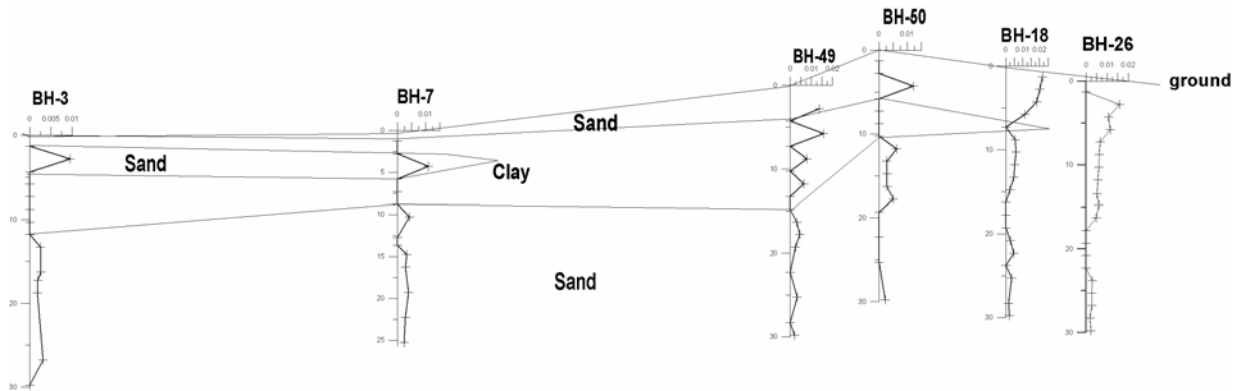


Fig. 10. The Soil and ALP Profile of D Section

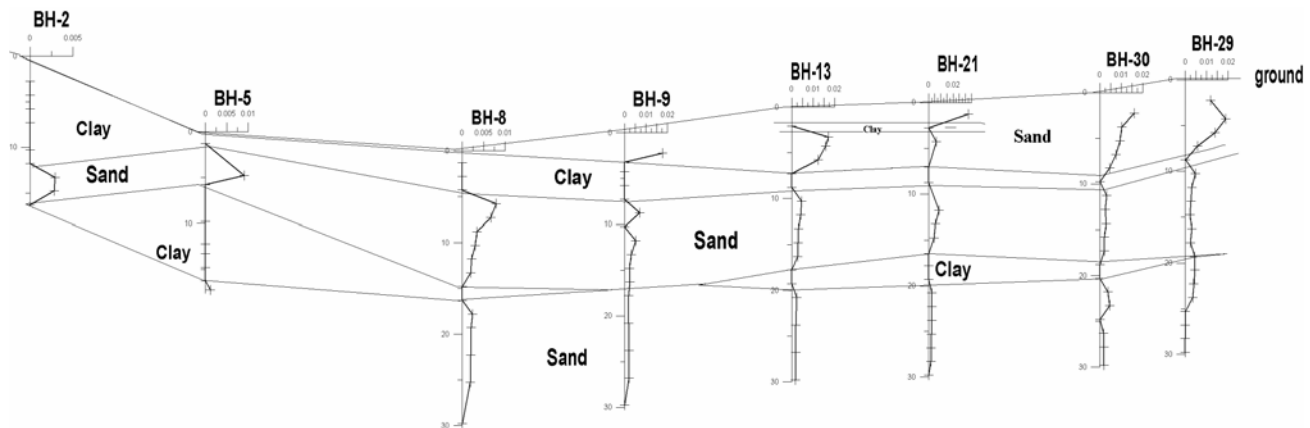


Fig. 11. The Soil and ALP Profile of E Section

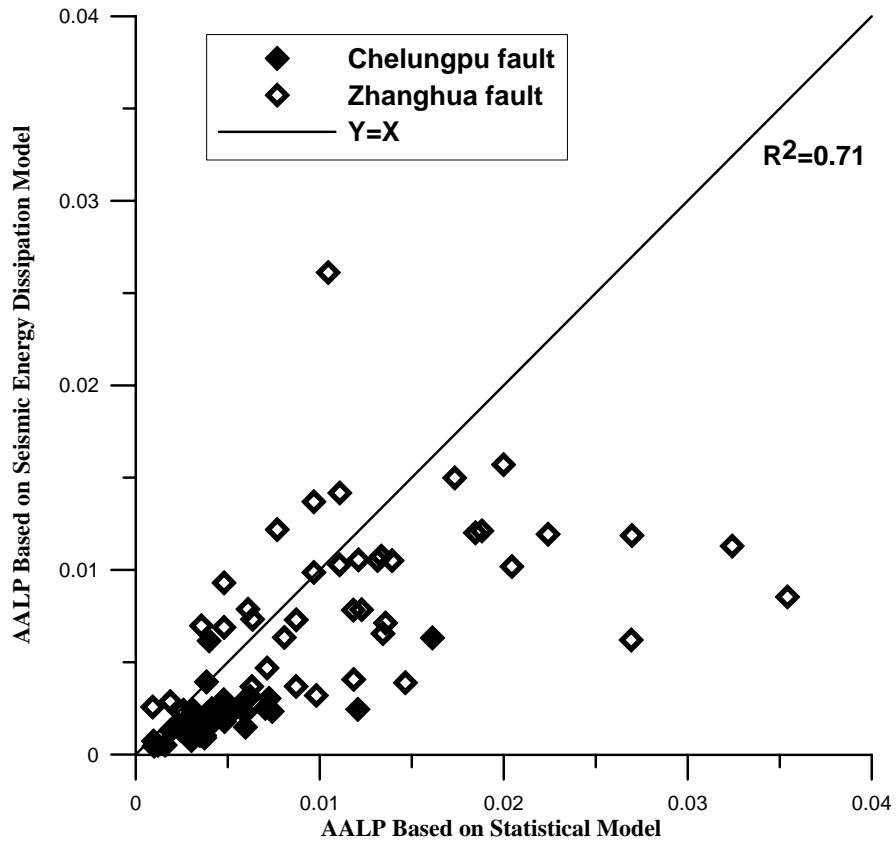


Fig.12 Relationship between Statistical Model and Seismic Energy Dissipation Model for AALP

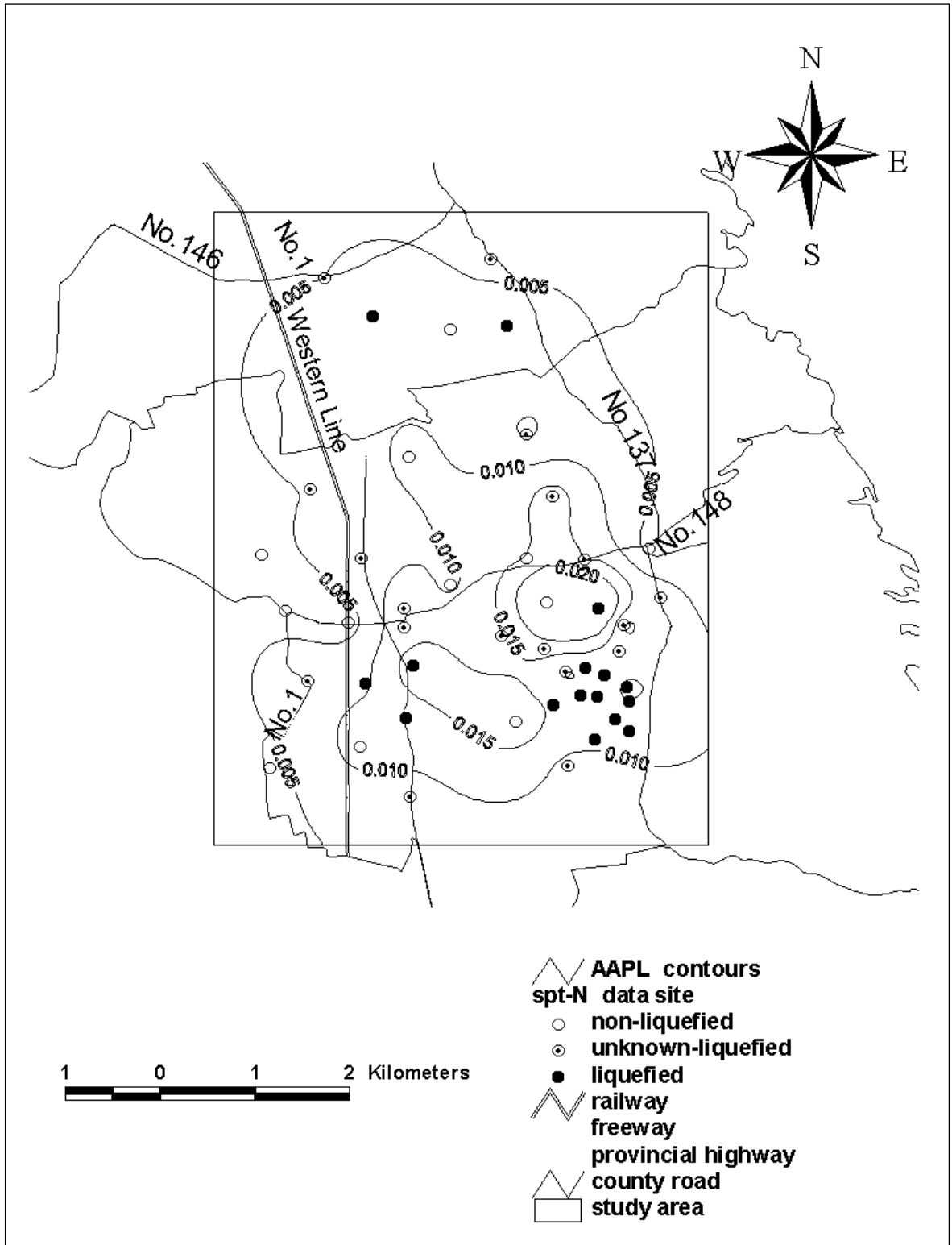


Fig.13 Map of AALP for Yunlin Area